

Title	Stoichiometry control and epitaxial growth of AgCrSe <sub>2</sub> thin films by pulsed-laser deposition
Author(s)	Tajima, Yusuke; Inamura, Kenshin; Masaki, Sebun et al.
Citation	APL Materials. 2025, 13(6), p. 061117
Version Type	VoR
URL	https://hdl.handle.net/11094/102925
rights	Copyright (2025) Author(s). This article is distributed under a Creative Commons Attribution (CC BY-NC) License.
Note	

### The University of Osaka Institutional Knowledge Archive : OUKA

https://ir.library.osaka-u.ac.jp/

The University of Osaka

RESEARCH ARTICLE | JUNE 11 2025

## Stoichiometry control and epitaxial growth of AgCrSe<sub>2</sub> thin films by pulsed-laser deposition

Yusuke Tajima; Kenshin Inamura ⑩ ; Sebun Masaki; Takumi Yamazaki ⑩ ; Takeshi Seki ⑩ ; Kazutaka Kudo ⑩ ; Jobu Matsuno ⑩ ; Junichi Shiogai ➡ ⑩



APL Mater. 13, 061117 (2025) https://doi.org/10.1063/5.0273060





### Articles You May Be Interested In

Interface design of transparent thermoelectric epitaxial ZnO/SnO<sub>2</sub> multilayer film for simultaneous realization of low thermal conductivity and high optical transmittance

Appl. Phys. Lett. (January 2023)

Non-coplanar spin structure in a metallic thin film of triangular lattice antiferromagnet CrSe

APL Mater. (April 2024)

Crystal-liquid duality driven ultralow two-channel thermal conductivity in  $\alpha\text{-MgAgSb}$ 

Appl. Phys. Rev. (January 2024)





# Stoichiometry control and epitaxial growth of AgCrSe<sub>2</sub> thin films by pulsed-laser deposition

Cite as: APL Mater. 13, 061117 (2025); doi: 10.1063/5.0273060

Submitted: 28 March 2025 • Accepted: 27 May 2025 •

Published Online: 11 June 2025







Yusuke Tajima,¹ Kenshin Inamura,¹ D Sebun Masaki,¹ Takumi Yamazaki,² D Takeshi Seki,²³ D Kazutaka Kudo.¹.⁴ D Jobu Matsuno.¹.⁴ D and Junichi Shiogai¹.4.a¹ D

### **AFFILIATIONS**

- Department of Physics, Osaka University, Toyonaka, Osaka 560-0043, Japan
- <sup>2</sup>Institute for Materials Research, Tohoku University, Sendai, Miyagi 980-8577, Japan
- Center for Science and Innovation in Spintronics, Tohoku University, Sendai, Miyagi 980-8577, Japan
- <sup>4</sup>Division of Spintronics Research Network, Institute for Open and Transdisciplinary Research Initiatives, Osaka University, Suita, Osaka 565-0871, Japan

#### **ABSTRACT**

We report on epitaxial growth in thin-film synthesis of a polar magnetic semiconductor, AgCrSe<sub>2</sub>, on a lattice-matched yttria-stabilized zirconia (111) substrate by pulsed-layer deposition (PLD). By using an Ag-rich PLD target to compensate for Ag deficiency in thin films, the nucleation of impurity phases is suppressed, resulting in the *c*-axis-oriented and single-phase AgCrSe<sub>2</sub> thin film. Structural analysis using x-ray diffraction and cross-sectional scanning transmission electron microscopy reveals epitaxial growth with the presence of both twisted and polar domains. Optical absorbance spectrum and magnetization measurements show an absorption edge at around 0.84 eV and a magnetic transition temperature at 41 K, respectively. These values are consistent with the reported values of direct bandgap and Néel temperature of bulk AgCrSe<sub>2</sub>, reflecting a single-phase and stoichiometric feature of the obtained film. Our demonstration of epitaxial thin-film growth of AgCrSe<sub>2</sub> serves as a bedrock for exploration of its potential thermoelectric and spintronic functionalities at surfaces or heterointerfaces.

© 2025 Author(s). All article content, except where otherwise noted, is licensed under a Creative Commons Attribution-NonCommercial 4.0 International (CC BY-NC) license (https://creativecommons.org/licenses/by-nc/4.0/). https://doi.org/10.1063/5.0273060

### I. INTRODUCTION

A ternary chromium compound, AgCrSe<sub>2</sub> (R3m), is a p-type and polar magnetic semiconductor. Its hexagonal crystal structure, with a and c-axis lengths being 3.680 and 21.225 Å, is composed of alternating stacking of two-dimensional (2D) networks of edgesharing CrSe<sub>6</sub> octahedra (referred to as CrSe<sub>2</sub> networks hereafter) and AgSe<sub>4</sub> tetrahedral layers,  $^{2.3}$  as shown in the left panel of Fig. 1(a). AgCrSe<sub>2</sub> and related family compounds ACrX<sub>2</sub> (A: monovalent ions, X: chalcogens) have recently attracted much interest in a wide range of realms because they exhibit unique structural and ionic properties related to A sublattices,  $^{4.5}$  and intriguing magnetic states  $^{6.7}$  and magneto-transport phenomena  $^{8.9}$  stemming from the Cr triangular lattice in the CrX<sub>2</sub> network. Previous powder x-ray diffraction (XRD) studies have revealed that AgCrSe<sub>2</sub> undergoes a second-order transition from a low-temperature ordered phase (R3m) to a high-temperature disordered phase [R3m, the right panel

of Fig. 1(a)] across a temperature around 475 K.3 This transition is related to disordering of Ag occupancy at the  $\alpha$  and  $\beta$  tetrahedral sites between the CrSe<sub>2</sub> networks [Fig. 1(b)]. In the low-temperature phase, the Ag occupies either the  $\alpha$  or  $\beta$  site and forms a nonbuckled one-atomic-layer 2D sheet. The tetrahedral coordination of Ag breaks inversion symmetry along the c axis and induces spontaneous polarization: three bonds are formed with upper Se atoms and one bond is formed with a lower Se atom when Ag occupies the  $\alpha$  site, as shown in Fig. 1(b). The polarization is inverted when Ag occupies the  $\beta$  site. The spontaneous polarization gives rise to the Rashba spin-orbit interaction, which induces spin-split metallic surface state on the CrSe<sub>2</sub> termination<sup>10</sup> or giant magnetoresistance in bulk.<sup>8</sup> In addition, S = 3/2 spin of  $Cr^{3+}$  within the  $CrSe_2$  network is regarded as a 2D triangular-lattice antiferromagnet with Néel temperature T<sub>N</sub> below 50 K in AgCrSe<sub>2</sub>, leading to exotic magnetic states such as cycloidal<sup>2,11</sup> or noncoplanar spin structures.<sup>6,12</sup> Actually, the Weiss temperature of around 75 K being higher than  $T_{\rm N}$  is

a) Author to whom correspondence should be addressed: junichi.shiogai.sci@osaka-u.ac.jp

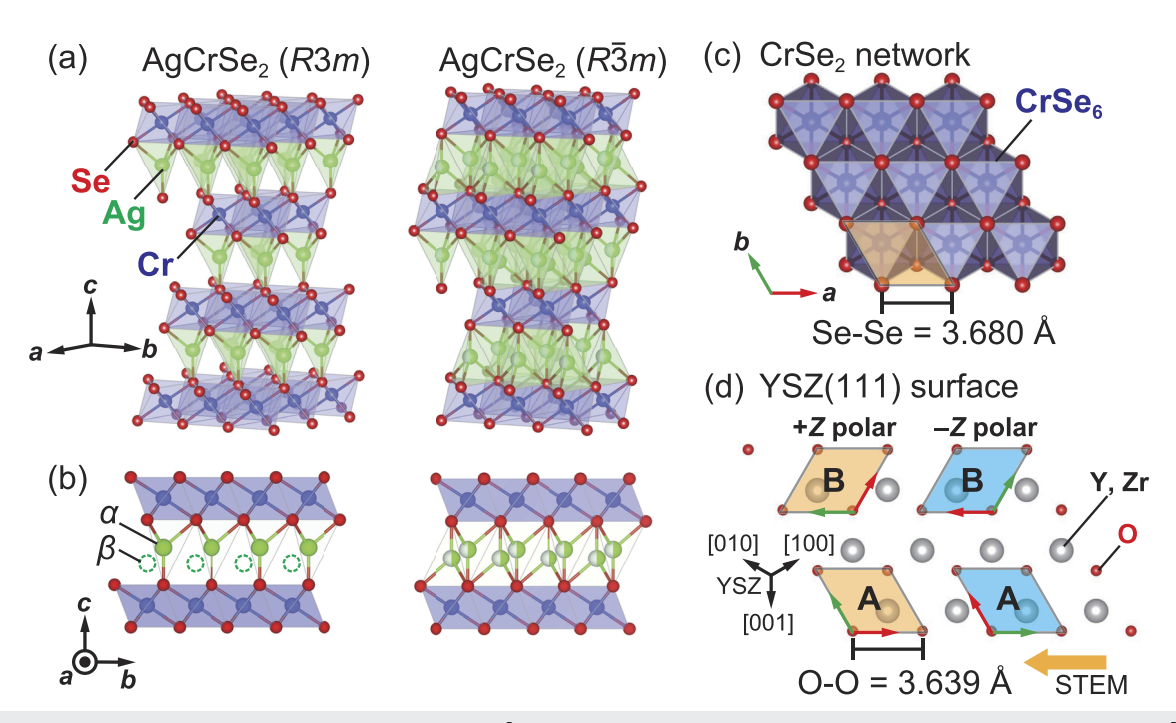


FIG. 1. (a) Schematic crystal structures of AgCrSe<sub>2</sub> in R3m (left) and  $R\bar{3}m$  (right) structures. (b) Side views of CrSe<sub>2</sub>/Ag/CrSe<sub>2</sub> stacks in R3m (left) and  $R\bar{3}m$  (right) structures. The green and white bicolor spheres represent the half occupancy at the Ag sites. (c) Top view of a single layer CrSe<sub>2</sub> two-dimensional network. The orange parallelogram represents a single unit-cell of the CrSe<sub>2</sub> network. (d) In-plane atomic arrangement of the topmost O atoms and Y or Zr atoms on the YSZ(111) surface. Orange parallelograms correspond to the possible arrangement of the CrSe<sub>2</sub> network with the epitaxial relationship in which the a axis of AgCrSe<sub>2</sub> is parallel to YSZ[1 $\bar{1}$ 0] (denoted as A domain) and YSZ[10 $\bar{1}$ 1] (denoted as B domain), and the c axis of AgCrSe<sub>2</sub> points in the +Z direction (+Z polar). Blue parallelograms represent A and B domains with the c axis of AgCrSe<sub>2</sub> pointing in the -Z direction (-Z polar). A horizontal orange arrow indicates observation direction in scanning transmission electron microscopy (STEM) imaging.

reported in AgCrSe<sub>2</sub> as a signature of spin frustration.<sup>6</sup> In the high-temperature phase, Ag occupies 50% of each site and forms a 2D buckled honeycomb lattice in the *ab* plane. Superionic behavior<sup>1,13</sup> and ultralow thermal conductivity,<sup>4</sup> linked to the disordering of Ag ions,<sup>5,14</sup> have been reported. On this basis, AgCrSe<sub>2</sub> is also a promising thermoelectric material.<sup>15,16</sup>

Considering that intensive studies of AgCrSe<sub>2</sub> in bulk and powder forms have revealed its high potential not only in fundamental spin-related physical phenomena but also for energy-harvesting applications, thin-film synthesis of AgCrSe<sub>2</sub> will make this family of compounds even more attractive in view of large-area applications, observation of quantum phenomena by electric-field gating<sup>17</sup> or amplifying surface effects,<sup>10</sup> as well as possible emergence of multiferroicity in the ultra-thin limit.<sup>18</sup> Yet, synthesis of single-phase AgCrSe<sub>2</sub> thin film remains challenging, probably because of difficulty in composition tuning owing to the highly volatile feature of Ag and the tendency for segregation of Cr–Se impurity phases.<sup>19</sup> In this study, we report on the synthesis of epitaxial and single-phase AgCrSe<sub>2</sub> thin film in pulsed-laser deposition (PLD) using an Ag-rich target, which we found allows compensating for Ag deficiency and suppressing the impurity phases.

Our previous work suggests that the (111) plane of yttriastabilized zirconia (YSZ: Fm3m) substrate is suitable for epitaxial thin-film growth of the CrSe<sub>2</sub> network.<sup>20</sup> On the CrSe<sub>2</sub> network of

AgCrSe2, the Se atoms of the CrSe6 octahedra form a triangular lattice as shown in Fig. 1(c), and the neighboring Se-Se distance is 3.680 Å.<sup>3</sup> Figure 1(d) illustrates the in-plane atomic arrangement of the topmost O atoms and underlying cations (Y or Zr) on YSZ(111) and considers possible epitaxial relationships, which are attributed to twisted and polar domains of AgCrSe<sub>2</sub> (R3m). The neighboring O-O distance of the top-most O plane on YSZ(111) is 3.639 Å, which closely matches the Se-Se distance with a small lattice mismatch of 1.1%. In the case that the c axis of AgCrSe<sub>2</sub> points upward (+Z polar, orange rhombus), the in-plane orientation of the Se triangular lattice consists of two possible configurations: the a axis of the CrSe<sub>2</sub> network [red arrow in Fig. 1(d)] is parallel to the [110] direction of YSZ(111) (denoted as A domain) and is rotated by 60° with the a axis being parallel to  $[10\overline{1}]$  of YSZ(111) (denoted as B domain). Despite the threefold symmetry around the c axis of AgCrSe<sub>2</sub> and [111] of YSZ(111), the twisted domains in thin film seem energetically degenerate owing to the structural similarity of the Se and O triangular lattices. The same argument was also given for the thinfilm growth of the similar compound, delafossite oxide PdCoO2 on the c-plane of the Al<sub>2</sub>O<sub>3</sub> substrate.<sup>21</sup> By comparing PdCoO<sub>2</sub> having O-Pd-O dumbbell-like bonding between the CoO2 networks, AgCrSe2 possesses an AgSe4 tetrahedral layer between the CrSe2 networks, which breaks inversion symmetry. Therefore, two extra configurations, which rely on this tetrahedral coordination, should

be considered for the low-temperature ordered phase: the c axis of AgCrSe<sub>2</sub> points upward (denoted as +Z polar) or downward (denoted as -Z polar, blue rhombus) as shown in Fig. 1(d). In the structural characterization of AgCrSe<sub>2</sub> thin film, these two degrees of freedom, in-plane rotation and polarization, are considered.

### II. EXPERIMENTAL METHODS

The 100-nm-thick thin-film samples were prepared on YSZ(111) substrates by pulsed-laser deposition at substrate temperature T<sub>sub</sub> ranging from 300 to 500°C. We used an Ag-rich AgCrSe<sub>2</sub> target for synthesizing stoichiometric thin films and a stoichiometric AgCrSe<sub>2</sub> target as a reference experiment. For synthesis of the PLD targets, we first prepared polycrystalline AgCrSe2 samples using a solid-state reaction. Stoichiometric amounts of the starting materials Ag (99.9%), Cr (99.99%), and Se (99.9%) (Kojundo Chemical Laboratory Co. Ltd.) were mixed, pressed into pellets, and then heated in an evacuated quartz tube at 800°C for 24 h twice with pulverizing and pressing in between. The resulting samples were characterized by means of powder x-ray diffraction (XRD) using an x-ray diffractometer (Rigaku MiniFlex600-C) with Cu-Kα radiation, equipped with a high-speed one-dimensional detector (Rigaku D/teX Ultra2), and it was confirmed that they consisted of single-phase AgCrSe<sub>2</sub>. The obtained polycrystalline AgCrSe<sub>2</sub> pellet was then used as the stoichiometric target. The Ag-rich target was prepared by grinding the stoichiometric AgCrSe2 samples, mixing them with commercially available Ag<sub>2</sub>Se (P2<sub>1</sub>2<sub>1</sub>2<sub>1</sub>) powder (Kojundo Chemical Laboratory Co. Ltd.) with a 2:1 molar ratio, and pressing them into a pellet. The resultant target consists of a mixture of AgCrSe2 and Ag2Se with the Ag/Cr atomic ratio of 2. The structural characterization of thin-film samples was performed by XRD (X'pert PRO MRD, PANalytical B.V.) with a Cu– $K\alpha_1$  x-ray source ( $\lambda = 1.5406$  Å) and cross-sectional scanning transmission electron microscopy (STEM) imaging using FEI-Titan G2-cubed (TU-503). The Ag/Cr chemical composition ratio of thin films was determined by energy dispersive x-ray spectroscopy (EDX) using a scanning electron microscope (Hitachi High-Tech TM4000Plus II) equipped with an energy dispersive spectrometer (Oxford Instruments AztecOne). The optical absorption spectrum of the AgCrSe2 thin film was obtained by the total reflectance measurement using an ultraviolet–visible spectrophotometer equipped with an integrating sphere (U-4100, HITACHI, Japan). Magnetization measurements were performed by a magnetic properties measurement system (MPMS3, Quantum Design, Inc.) with a typical sample area of about 3  $\times$  3 mm². Schematics of crystal structure, in-plane atomic arrangements, and cross-sectional structural patterns were drawn with VESTA3.  $^{22}$ 

### III. RESULTS AND DISCUSSION

### A. Optimization of growth condition for single-crystalline AgCrSe<sub>2</sub> thin film

We first optimize growth conditions for the synthesis of single-phase AgCrSe<sub>2</sub> thin films. Figure 2(a) shows a 2theta-theta scan of the XRD patterns of the AgCrSe<sub>2</sub> thin films grown at  $T_{\rm sub}=450$  and  $500^{\circ}$ C using the stoichiometric AgCrSe<sub>2</sub> target (black lines) and those grown at  $T_{\rm sub}=400$ , 425, 450, 475, and  $500^{\circ}$ C using the Ag-rich target. The main diffraction peaks commonly observed for all the films are identified as diffraction from AgCrSe<sub>2</sub>(003*I*), indicating the *c*-axis-oriented growth of the *R3m* structure since the low-angle (003) and (006) diffraction peaks are prohibited for the  $R\bar{3}m$  structure. <sup>4.5</sup> For the films using a stoichiometric target, the larger intensities of the (003) and (0012) diffraction peaks of Cr<sub>2</sub>Se<sub>3</sub> than (003*I*) of AgCrSe<sub>2</sub> are observed, indicating the presence of a significant volume fraction of the Cr<sub>2</sub>Se<sub>3</sub> phase. Such segregation of

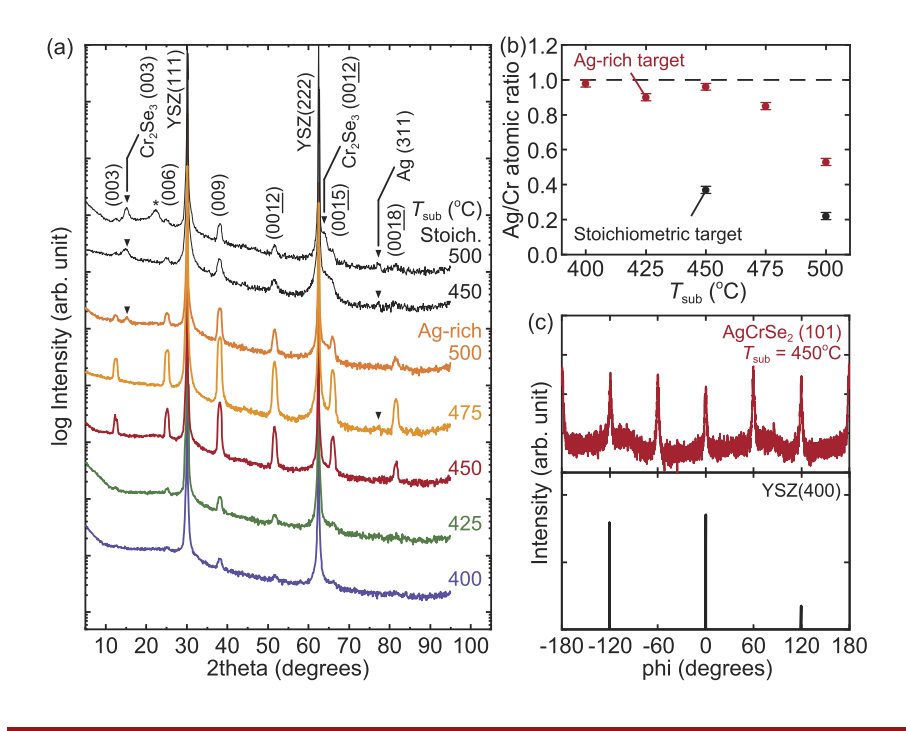


FIG. 2. (a) 2theta-theta scan of the xray diffraction (XRD) patterns for  $T_{sub}$ = 450 and 500°C using stoichiometric AgCrSe2 target (black lines) and those grown at  $T_{\text{sub}} = 400$  (purple), 425 (green), 450 (red), 475 (light orange), and 500°C (orange) using Ag-rich target. The asterisk (\*) denotes the peak originating from the sample holder. (b) Ag/Cr atomic ratio on the thin films as a function of T<sub>sub</sub> using stoichiometric (black) and Ag-rich (red) targets. The error bars were estimated from the standard deviations of the Ag/Cr ratio in the different areas of the identical samples. A horizontal dashed line indicates Ag/Cr = 1. (c) In-plane phi-scan of XRD patterns of AgCrSe<sub>2</sub>(101) (top panel) and YSZ(400) (bottom panel).

APL Materials ARTICLE pubs.aip.org/aip/apm

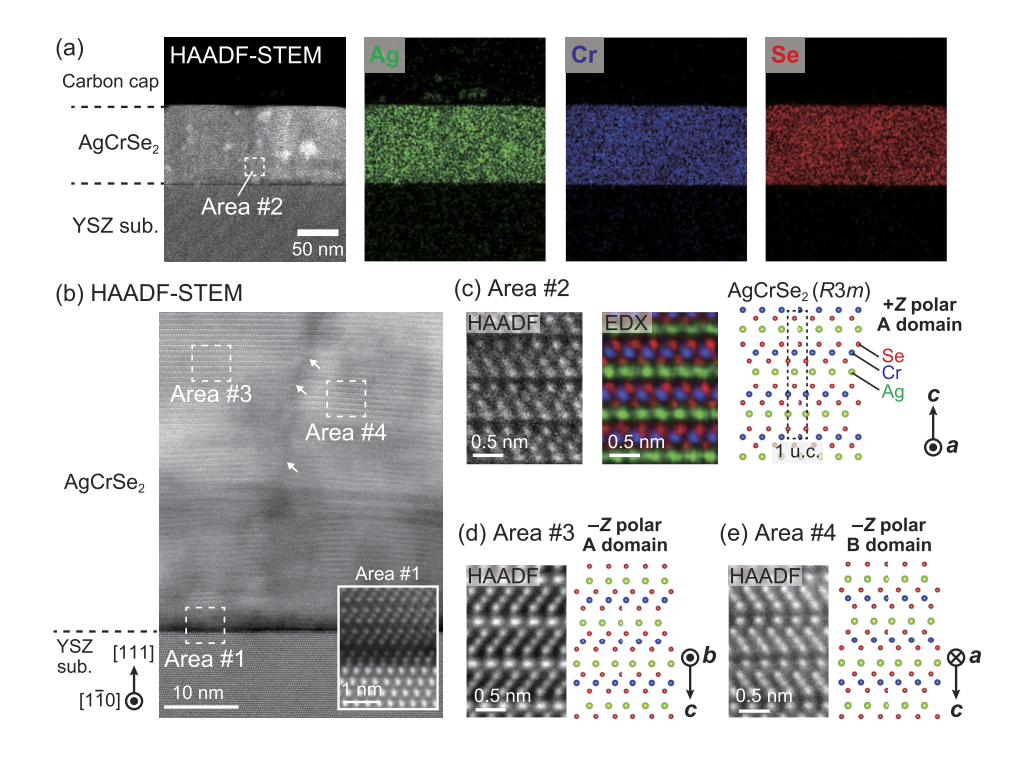


FIG. 3. (a) Wide-view high-angle annular dark field (HAADF) scanning transmission electron micrograph (STEM) image and elemental distribution mapping of the AgCrSe<sub>2</sub> thin film grown on YSZ(111) taken from YSZ[110]. (b) High-resolution HAADF-STEM image of the AgCrSe2 film. White arrows indicate a boundary between twisted domains. (Inset) An atomically resolved HAADF-STEM image around AgCrSe2/YSZ interface (Area #1). (c) An atomically resolved HAADF-STEM image and EDX elemental mapping in Area #2, and corresponding cross-sectional structural pattern of the R3m structure viewed from the a axis of AgCrSe<sub>2</sub> (+Z polar A domain). (d) (e) Atomically resolved HAADF-STEM images for Areas #3 and #4 and corresponding structural patterns viewed from the b axis of AgCrSe2 (-Z polar A domain) and along the a axis (-Z polar)B domain), respectively.

the Cr<sub>2</sub>Se<sub>3</sub> phase was reported in previous thin-film studies using molecular beam epitaxy, and the emergence of this Ag-deficient impurity phase was attributed to the high volatility of Ag. 19 The Agdeficient phase is a common impurity in AgCrSe2 in both bulk and thin films. 19,23 In addition, a weak Ag(331) peak was also observed around 2theta ~78 degrees. This may be caused by the aggregation of Ag expelled from the Ag-deficient phase. With the aim of suppressing the Cr<sub>2</sub>Se<sub>3</sub> phase, we employed the Ag-rich target to compensate for the Ag deficiency. At  $T_{\text{sub}} = 400^{\circ}\text{C}$  [purple line in Fig. 2(a)], the weak diffraction peaks of AgCrSe<sub>2</sub> are observed, while those of  $Cr_2Se_3$  are not detected. With increasing  $T_{sub}$  up to  $450^{\circ}C$ [red line in Fig. 2(a)], the intensity of the AgCrSe<sub>2</sub> peaks becomes stronger than those for 400 and 425°C while keeping the absence of the impurity phases. With further increasing  $T_{\rm sub}$  to 475 and 500 $^{\circ}$ C [light and dark orange lines in Fig. 2(a)], the impurity peaks start to appear. The c-axis length determined by the (009) peak is 21.226  $\pm$  0.005 Å, which shows no systematic variation among samples prepared with different  $T_{\text{sub}}$  and is almost consistent with the bulk value (c = 21.225 Å). Figure 2(b) shows the  $T_{\text{sub}}$  dependence of the Ag/Cr composition ratio for the thin films fabricated from the stoichiometric and Ag-rich PLD targets. In the whole T<sub>sub</sub> range, the Ag/Cr ratio is smaller for the stoichiometric target than that for the Ag-rich target. In addition, with increasing  $T_{\text{sub}}$ , the Ag/Cr ratio for the Ag-rich target starts to decrease in  $T_{\text{sub}} \ge 475^{\circ}\text{C}$ , which can be explained by the high volatility of Ag and is consistent with the emergence of the  $Cr_2Se_3$  phase in thin films grown at high  $T_{sub}$ , as shown in Fig. 2(a). The stoichiometric composition of AgCrSe<sub>2</sub> is obtained at  $T_{\text{sub}} \le 450^{\circ}\text{C}$  [a horizontal dashed line in Fig. 2(b)] only when using the Ag-rich target, which is also consistent with the single phase AgCrSe<sub>2</sub> in this growth condition as judged by XRD. Based on these observations, we conclude that  $T_{\rm sub} = 450^{\circ}{\rm C}$  is the optimal growth temperature for obtaining the single-phase AgCrSe<sub>2</sub> thin film when using the Ag-rich target with an Ag/Cr ratio of 2. The optimal  $T_{\rm sub}$  could be made higher by using the target containing a higher fraction of Ag<sub>2</sub>Se. Hereafter, further structural and physical property characterizations were performed for the AgCrSe<sub>2</sub> thin film grown at  $T_{\rm sub} = 450^{\circ}{\rm C}$  with the Ag-rich target.

Figure 2(c) shows the in-plane phi-scan XRD pattern of AgCrSe<sub>2</sub>(101) and YSZ(400) diffraction peaks. Threefold in-plane rotational symmetry is exhibited in YSZ(400), being consistent with the  $C_3$  symmetry around the [111] axis on YSZ(111). On the other hand, we observe sixfold peaks for AgCrSe<sub>2</sub>(101) every 60°, despite that the [001] axis of the R3m structure is the  $C_3$  symmetry. The a-axis length of 3.682 Å extracted from AgCrSe<sub>2</sub>(101) is consistent with the bulk value (a = 3.680 Å). From these in-plane XRD patterns, we conclude that the c-axis-oriented AgCrSe<sub>2</sub> thin film contains two twisted domains rotated by 60° around the c axis with the epitaxial relationship in which the a axis of AgCrSe<sub>2</sub> is parallel to YSZ[1 $\bar{1}$ 0] (A domain) and YSZ[10 $\bar{1}$ 1] (B domain), as discussed in Fig. 1(d).

### B. Structural characterization using atomically resolved STEM imaging

Cross-sectional STEM imaging provides further microscopic insights into the formation of the single-phase R3m structure of AgCrSe<sub>2</sub> as well as crystal orientation. A viewing orientation, as depicted by an orange arrow in Fig. 1(d), was chosen opposite to the  $[1\bar{1}0]$  direction of YSZ(111) because the  $[1\bar{1}0]$  direction should be parallel to either the a or b axis of AgCrSe<sub>2</sub> so that we can identify the

Ag ion location between CrSe<sub>2</sub> layers, as shown in Fig. 1(b). We first investigate elemental distribution in a wide area of cross-sectional high angle annular dark field (HAADF) STEM image in Fig. 3(a) for the AgCrSe2 thin film on the YSZ substrate. Uniform distributions of Ag, Cr, and Se with no segregation are demonstrated, being consistent with the XRD observation. Figure 3(b) shows a magnified HAADF-STEM image, taken a few tens of  $\mu$ m away from Fig. 1(a), which consists of a grain boundary as indicated by white arrows. The *c*-axis-oriented layered structure of AgCrSe<sub>2</sub> is clearly seen over the film region. The inset in Fig. 3(b) shows an atomically resolved HAADF-STEM image around the film/substrate interface (Area #1), indicating the epitaxial growth of AgCrSe2 on the lattice-matched YSZ(111) substrate with a sharp interface. Note that the Ag layer is not clearly visible in the vicinity of the interface. This is possibly caused by large displacement and aggregation of Ag occurring after preparation of the STEM sample using a focused ion beam, as reported in Ge/Ag multilayers.<sup>24</sup> Another possibility is the preferential formation of an Ag-deficient CrSe2 initial layer on the YSZ substrate during thin-film growth. Figure 3(c) shows the atomically resolved HAADF-STEM image and EDX elemental mapping of Area #2 [indicated in Fig. 3(a)], as one of the representative patterns, and compares them with the simulated cross-sectional structural patterns. The HAADF-STEM and EDX mapping show the presence of a non-buckled Ag monolayer between the CrSe2 networks, being consistent with the R3m structure of AgCrSe2. Considering the location of Ag sites, the atomic structure of Area #2 is well reproduced by the structural pattern assuming +Z polar and A domain defined in Fig. 1(d). Figures 3(d) and 3(e) compare the HAADF-STEM images taken around two areas (Areas #3 and #4) across the grain boundary together with corresponding simulated structural patterns. The atomic arrangements of the CrSe2 networks and Ag layers in between Areas #3 and #4 show mirror-symmetric patterns, corresponding to the 60°-twisted domain with the common polar direction. By considering the location of Ag, the HAADF-STEM images are consistent with the structural pattern simulating -Z polar and A domain for Area #3 [Fig. 3(d)] and -Z polar and B domain for Area #4 [Fig. 3(e)], respectively. Piezo-response force microscopy or polarized optical microscopy will provide further quantitative characterization of the polar domains. Although we found the use of lattice-matched YSZ(111) substrate and Agrich target is effective for obtaining single-phase epitaxial AgCrSe2 thin film, further improvement in the synthesis process is needed for single-domain films. For example, using facet-controlled substrates<sup>25</sup> or polar substrates<sup>26</sup> may be useful for lifting in-plane degeneracy.

### C. Optical bandgap and magnetic transition temperature of AgCrSe<sub>2</sub> thin film

The physical properties of the single-phase  $AgCrSe_2$  thin film were characterized in view of optical bandgap  $E_g$  and Néel temperature  $T_N$ . A previous study of Hall measurements in bulk experiments reported that  $AgCrSe_2$  is a p-type semiconductor with a bandgap of 0.5 eV, while density-functional theory calculations suggest direct and indirect bandgaps of 0.7 and 0.1 eV, respectively. The  $E_g$  value of the  $AgCrSe_2$  thin film was estimated from the absorbance spectrum [A(hv)] spectrum with hv being photon energy] collected in total reflectance measurements. Figure 4(a) shows A(hv) spectra for

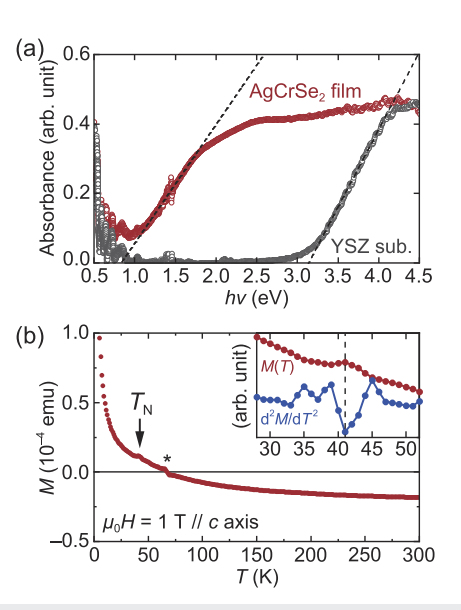


**FIG. 4.** (a) Optical absorbance spectra for AgCrSe $_2$  film on YSZ(111) substrate (red) and reference YSZ substrate (gray) obtained from total reflectance measurements. (b) Temperature dependence of magnetization [M(T) curve] of AgCrSe $_2$  film on YSZ(111) substrate. The  $T_N$  and asterisk (\*) denote Néel temperature and the temperature where M(T) crosses zero, respectively. (Inset) M(T) and its second derivative around  $T_N$ .

the AgCrSe<sub>2</sub> thin film on the YSZ(111) substrate (red) and the reference YSZ(111) substrate (gray). An extrapolation to the A(hv) spectrum of the YSZ substrate around the absorption edge yields  $E_{\rm g} \sim 3$  eV, which is consistent with previous report, <sup>27</sup> suggesting the validity of the experimental setup. For the AgCrSe<sub>2</sub> thin film, a clear absorption edge in hv > 1 eV is observed. An extrapolation of the A(hv) spectrum in the linear region of 1.2 eV < hv < 1.7 eV yields an  $E_{\rm g}$  of 0.84 eV, which is roughly consistent with the previous report.<sup>8</sup>

Figure 4(b) shows the temperature dependence of magnetization [M(T)] curve of AgCrSe<sub>2</sub> thin film on YSZ substrate measured in an out-of-plane magnetic field of  $\mu_0 H = 1$  T after 7 T field cooling in the range of 5 K < T < 300 K. The overall M(T) consists of a negative component in the high-temperature range and a positive component sharply increasing with decreasing T in the low-temperature range, which we assigned to the diamagnetic and paramagnetic contributions of the YSZ substrate, respectively [see supplementary material, Fig. S1]. In addition to the substrate contributions, a clear hump around  $T \sim 41$  K is observed, as highlighted by the vertical dashed line in the inset of Fig. 4(b). This hump structure is absent in the M(T) curve of the reference substrate (see inset of Fig. S1). By considering the reported value of  $T_N \sim 45$  K for the bulk  $AgCrSe_2$ , we ascribed the observed hump in the M(T) curve of the AgCrSe2 thin film as a development of antiferromagnetic order. The observation of comparable values of  $E_g$  and  $T_N$  with bulk reflects the single-phase and stoichiometric features of the obtained AgCrSe<sub>2</sub> thin film.

#### IV. SUMMARY AND OUTLOOK

In summary, we have obtained an epitaxial and single-phase AgCrSe<sub>2</sub> thin film on a lattice-matched YSZ(111) substrate by

employing an Ag-rich target and precisely tuning the growth temperature to suppress Ag-deficient impurity phases. The XRD analysis reveals the presence of two in-plane twisted domains rotated by 60° with comparable volume fractions. In addition, the atomically resolved STEM imaging shows lattice-matched epitaxial growth as well as the presence of polar domains. Optical absorbance spectrum and magnetization measurements suggest that the optical bandgap and Néel temperature of the AgCrSe2 thin film are comparable to those of bulk, being consistent with the single-phase and stoichiometric features of the AgCrSe2 thin film. Our demonstration of epitaxial thin-film growth of AgCrSe2 tailors a platform to explore its potential functionalities based on thermoelectric, spintronic, or multiferroic thin-film devices.

### SUPPLEMENTARY MATERIAL

See the supplementary material for the temperature dependence of the magnetization curve of the reference YSZ substrate.

### **ACKNOWLEDGMENTS**

STEM observations and analyses were conducted with the cooperation of Koji Hayasaka, Makoto Nagasako, and Toyohiko J. Konno of Analytical Research Core for Advanced Materials, Institute for Materials Research, Tohoku University. This work was partly supported by the Tohoku University Microstructural Characterization Platform in MEXT Advanced Research Infrastructure for Materials and Nanotechnology in Japan (Grant No. JPMXP1224TU0205) and performed under the GIMRT Program of the Institute for Materials Research, Tohoku University (Proposal No. 202312-CRKEQ-0033). Total reflectance measurements were performed using research equipment shared in the MEXT Project for promoting public utilization of advanced research infrastructure (Program for supporting construction of core facilities), Grant No. JPMXS0441200024. This work was supported by JST, PRESTO Grant Nos. JPMJPR21A8 and JSPS KAKENHI, Grant Nos. JP23H01686, JP23K26379, JP22H01182, JP23K22453, and JP24K21531, and the Tanikawa Foundation.

### **AUTHOR DECLARATIONS**

### **Conflict of Interest**

The authors have no conflicts to disclose.

### **Author Contributions**

Yusuke Tajima and Kenshin Inamura contributed equally to this paper.

Yusuke Tajima: Data curation (lead); Formal analysis (equal); Visualization (equal); Writing – original draft (equal). Kenshin Inamura: Data curation (equal); Formal analysis (equal); Writing – original draft (equal). Sebun Masaki: Resources (equal); Writing – review & editing (equal). Takumi Yamazaki: Resources (equal); Writing – review & editing (equal). Takeshi Seki: Resources (equal); Writing – review & editing (equal). Kazutaka Kudo: Resources (equal); Writing – review & editing (equal). Jobu Matsuno: Supervision (lead); Writing – review & editing (equal).

**Junichi Shiogai**: Conceptualization (lead); Visualization (equal); Writing – original draft (equal).

### **DATA AVAILABILITY**

The data that support the findings of this study are available from the corresponding author upon reasonable request.

#### REFERENCES

- <sup>1</sup>B. A. Boukamp and G. A. Wiegers, "Ionic and electronic processes in AgCrSe<sub>2</sub>," Solid State Ionics **9–10**, 1193 (1983).
- <sup>2</sup>P. F. Bongers, C. F. van Bruggen, J. Koopstra, W. P. F. A. M. Omloo, G. A. Wiegers, and F. Jellinek, "Structures and magnetic properties of some metal (I) chromium (III) sulfides and selenides," J. Phys. Chem. Solids **29**, 977 (1968).
- <sup>3</sup> A. van der Lee and G. A. Wiegers, "Anharmonic thermal motion of Ag in AgCrSe<sub>2</sub>: A high-temperature single-crystal X-ray diffraction study," J. Solid State Chem. **82**, 216 (1989).
- <sup>4</sup>B. Li, H. Wang, Y. Kawakita, Q. Zhang, M. Feygenson, H. L. Yu, D. Wu, K. Ohara, T. Kikuchi, K. Shibata, T. Yamada, X. K. Ning, Y. Chen, J. Q. He, D. Vaknin, R. Q. Wu, K. Nakajima, and M. G. Kanatzidis, "Liquid-like thermal conduction in intercalated layered crystalline solids," Nat. Mater. 17, 226 (2018).
- <sup>5</sup>J. Ding, J. L. Niedziela, D. Bansal, J. Wang, X. He, A. F. May, G. Ehlers, D. L. Abernathy, A. Said, A. Alatas, Y. Ren, G. Arya, and O. Delaire, "Anharmonic lattice dynamics and superionic transition in AgCrSe<sub>2</sub>," Proc. Natl. Acad. Sci. U. S. A. 117, 3930 (2020).
- <sup>6</sup>M. Baenitz, M. M. Piva, S. Luther, J. Sichelschmidt, K. M. Ranjith, H. Dawczak-Dębicki, M. O. Ajeesh, S. J. Kim, G. Siemann, C. Bigi, P. Manuel, D. Khalyavin, D. A. Sokolov, P. Mokhtari, H. Zhang, H. Yasuoka, P. D. C. King, G. Vinai, V. Polewczyk, P. Torelli, J. Wosnitza, U. Burkhardt, B. Schmidt, H. Rosner, S. Wirth, H. Kühne, M. Nicklas, and M. Schmidt, "Planar triangular S = 3/2 magnet AgCrSe<sub>2</sub>: Magnetic frustration, short range correlations, and field-tuned anisotropic cycloidal magnetic order," Phys. Rev. B **104**, 134410 (2021).
- <sup>7</sup>S. Kobayashi, H. Ueda, C. Michioka, and K. Yoshimura, "Competition between the direct exchange interaction and superexchange interaction in layered compounds LiCrSe<sub>2</sub>, LiCrTe<sub>2</sub>, and NaCrTe<sub>2</sub> with a triangular lattice," Inorg. Chem. 55, 7407–7413 (2016).
- <sup>8</sup>H. Takahashi, T. Akiba, A. H. Mayo, K. Akiba, A. Miyake, M. Tokunaga, H. Mori, R. Arita, and S. Ishiwata, "Spin-orbit-derived giant magnetoresistance in a layered magnetic semiconductor AgCrSe<sub>2</sub>," Phys. Rev. Mater. **6**, 054602 (2022).
- <sup>9</sup>H. Takatsu, S. Yonezawa, S. Fujimoto, and Y. Maeno, "Unconventional anomalous Hall effect in the metallic triangular-lattice magnet," Phys. Rev. Lett. **105**, 137201 (2010).
- <sup>10</sup>G. R. Siemann, S. J. Kim, E. A. Morales, P. A. E. Murgatroyd, A. Zivanovic, B. Edwards, I. Marković, F. Mazzola, L. Trzaska, O. J. Clark, C. Bigi, H. Zhang, B. Achinuq, T. Hesjedal, M. D. Watson, T. K. Kim, P. Bencok, G. van der Laan, C. M. Polley, M. Leandersson, H. Fedderwitz, K. Ali, T. Balasubramanian, M. Schmidt, M. Baenitz, H. Rosner, and P. D. C. King, "Spin-orbit coupled spin-polarised hole gas at the CrSe<sub>2</sub>-terminated surface of AgCrSe<sub>2</sub>," npj Quantum Mater. 8, 61 (2023).
- <sup>11</sup>F. M. R. Engelsman, G. A. Wiegers, F. Jellinek, and B. van Laar, "Crystal structures and magnetic structures of some metal(I) chromium(III) sulfides and selenides," J. Solid State Chem. **6**, 574 (1973).
- <sup>12</sup>Y. Tajima, J. Shiogai, K. Ueda, H. Suzaki, K. Takaki, T. Seki, K. Kudo, and J. Matsuno, "Non-coplanar spin structure in a metallic thin film of triangular lattice antiferromagnet CrSe," APL Mater. 12, 041112 (2024).
- <sup>13</sup>D. W. Murphy, H. S. Chen, and B. Tell, "Superionic conduction in AgCrS<sub>2</sub> and AgCrSe<sub>2</sub>," J. Electrochem. Soc. **124**, 1268 (1977).
- <sup>14</sup>F. Damay, S. Petit, S. Rols, M. Braendlein, R. Daou, E. Elkaïm, F. Fauth, F. Gascoin, C. Martin, and A. Maignan, "Localised Ag<sup>+</sup> vibrations at the origin of ultralow thermal conductivity in layered thermoelectric AgCrSe<sub>2</sub>," Sci. Rep. 6, 23415 (2016).

- <sup>15</sup>F. Gascoin and A. Maignan, "Order-Disorder transition in AgCrSe<sub>2</sub>: A new route to efficient thermoelectrics," Chem. Mater. 23, 2510 (2011).
- <sup>16</sup>A. Maignan, E. Guilmeau, F. Gascoin, Y. Bréard, and V. Hardy, "Revisiting some chalcogenides for thermoelectricity," Sci. Technol. Adv. Mater. 13, 053003 (2012).
- <sup>17</sup>S. J. Kim, J. Zhu, M. M. Piva, M. Schmidt, D. Fartab, A. P. Mackenzie, M. Baenitz, M. Nicklas, H. Rosner, A. M. Cook, R. González-Hernández, L. Šmejkal, and H. Zhang, "Observation of the anomalous Hall effect in a layered polar semiconductor," Adv. Sci. 11, 2307306 (2024).
- <sup>18</sup> Z. Sun, Y. Su, A. Zhi, Z. Gao, X. Han, K. Wu, L. Bao, Y. Huang, Y. Shi, X. Bai, P. Cheng, L. Chen, K. Wu, X. Tian, C. Wu, and B. Feng, "Evidence for multiferroicity in single-layer CuCrSe<sub>2</sub>," Nat. Commun. 15, 4252 (2024).
- <sup>19</sup>Y. Nanao, C. Bigi, A. Rajan, G. Vinai, D. Dagur, and P. D. C. King, "Epitaxial growth of AgCrSe<sub>2</sub> thin films by molecular beam epitaxy," J. Appl. Phys. 135, 045303 (2024).
- <sup>20</sup>Y. Tajima, J. Shiogai, M. Ochi, K. Kudo, and J. Matsuno, "Engineered substrates for domain control in CrSe thin-film growth: Single-domain formation on lattice-matched YSZ(111) substrate," Jpn. J. Appl. Phys. (in press) (2025).
- $^{21}$  T. Harada, K. Fujiwara, and A. Tsukazaki, "Highly conductive PdCoO $_2$ ultrathin films for transparent electrodes," APL Mater. **6**, 046107 (2018).

<sup>22</sup>K. Momma and F. Izumi, "VESTA 3 for three-dimensional visualization of crystal, volumetric and morphology data," J. Appl. Crystallogr. 44, 1272 (2011).

pubs.aip.org/aip/apm

- <sup>23</sup> M. Tang, Z. Chen, C. Yin, L. Lin, D. Ren, B. Liu, B. Kang, and R. Ang, "Thermoelectric modulation by intrinsic defects in superionic conductor Ag<sub>x</sub>CrSe<sub>2</sub>," Appl. Phys. Lett. **116**, 163901 (2020).
- <sup>24</sup>T. J. Konno and R. Sinclair, "Metal-mediated crystallization of amorphous germanium in germanium-silver layered systems," Philos. Mag. B 71, 179 (1995)
- <sup>25</sup> N. V. Tarakina, S. Schreyeck, M. Luysberg, S. Grauer, C. Schumacher, G. Karczewski, K. Brunner, C. Gould, H. Buhmann, R. E. Dunin-Borkowski, and L. W. Molenkamp, "Suppressing twin formation in Bi<sub>2</sub>Se<sub>3</sub> thin films," Adv. Mater. Interfaces 1, 1400134 (2014).
- $^{\bf 26}$  K. Fujiwara, H. Minato, J. Shiogai, A. Kumamoto, N. Shibata, and A. Tsukazaki, "Thin-film stabilization of LiNbO3-type ZnSnO3 and MgSnO3 by molecular-beam epitaxy," APL Mater. 7, 022505 (2019).
- $^{27}$ W. S. Choi, D. G. Kim, S. S. A. Seo, S. J. Moon, D. Lee, J. H. Lee, H. S. Lee, D. Y. Cho, Y. S. Lee, P. Murugavel, J. Yu, and T. W. Noh, "Electronic structures of hexagonal  $RMnO_3$  (R=Gd, Tb, Dy, and Ho) thin films: Optical spectroscopy and first-principles calculations," Phys. Rev. B 77, 045137 (2008).